Title

Nerve-targeted probes for fluorescence-guided intraoperative imaging

Journal

Theranostics, 8(15)

ISSN

1838-7640

Authors

Hingorani, Dina V
Whitney, Michael A
Friedman, Beth
et al.

Publication Date

2018

DOI

10.7150/thno.23084

Peer reviewed

IVYSPRING INTERNATIONAL PUBLISHER

Theranostics

2018; 8(15): 4226-4237. doi: 10.7150/thno.23084

Research Paper

Nerve-targeted probes for fluorescence-guided intraoperative imaging

Dina V Hingorani[1,3,*], Michael A Whitney[2,*], Beth Friedman[2], Joong-Keun Kwon[5], Jessica L Crisp[3], Qing Xiong[3], Larry Gross[3], Christopher J Kane[4], Roger Y Tsien[2,3,#] and Quyen T Nguyen[1,2]✉

1. Department of Surgery, Division of Otolaryngology-Head and Neck Surgery, University of California at San Diego, La Jolla, California, USA
2. Department of Pharmacology, University of California at San Diego, La Jolla, California, USA.
3. Howard Hughes Medical Institute, University of California at San Diego, La Jolla, California, USA
4. Department of Urology, UC San Diego Health System, La Jolla, California, USA.
5. Department of Otorhinolaryngology, Ulsan University Hospital, University of Ulsan College of Medicine, Ulsan, Republic of Korea

*Authors contributed equally

Author is deceased

✉ Corresponding author: Quyen T. Nguyen MD/PhD, UC San Diego MC 0647, 9500 Gilman Drive, La Jolla, CA 92093-0647. q1nguyen@ucsd.edu; Fax: (858)534-5270

Received: 2017.09.28; Accepted: 2018.04.27; Published: 2018.07.30

Abstract

A fundamental goal of many surgeries is nerve preservation, as inadvertent injury can lead to patient morbidity including numbness, pain, localized paralysis and incontinence. Nerve identification during surgery relies on multiple parameters including anatomy, texture, color and relationship to surrounding structures using white light illumination. We propose that fluorescent labeling of nerves can enhance the contrast between nerves and adjacent tissue during surgery which may lead to improved outcomes.

Methods: Nerve binding peptide sequences including HNP401 were identified by phage display using selective binding to dissected nerve tissue. Peptide dye conjugates including FAM-HNP401 and structural variants were synthesized and screened for nerve binding after topical application on fresh rodent and human tissue and in-vivo after systemic IV administration into both mice and rats. Nerve to muscle contrast was quantified by measuring fluorescent intensity after topical or systemic administration of peptide dye conjugate.

Results: Peptide dye conjugate FAM-HNP401 showed selective binding to human sural nerve with 10.9x fluorescence signal intensity (1374.44 ± 425.96) compared to a previously identified peptide FAM-NP41 (126.17 ± 61.03). FAM-HNP401 showed nerve-to-muscle contrast of 3.03 ± 0.57. FAM-HNP401 binds and highlight multiple human peripheral nerves including lower leg sural, upper arm medial antebrachial as well as autonomic nerves isolated from human prostate.

Conclusion: Phage display has identified a novel peptide that selectively binds to ex-vivo human nerves and in-vivo using rodent models. FAM-HNP401 or an optimized variant could be translated for use in a clinical setting for intraoperative identification of human nerves to improve visualization and potentially decrease the incidence of intra-surgical nerve injury.

Key words: human nerve, fluorescence imaging, nerve targeting, translational

Introduction

A fundamental goal of surgery is preservation of nerve function to minimize patient morbidity. Current nerve identification during surgery utilizes non-quantifiable criteria such as anatomy, texture, color and relationship to surrounding structures. In instances of trauma, tumor invasion or infection,

nerve identification using the above criteria can be even more challenging. Using white light reflectance, the visual difference between nerves, especially small nerves like the autonomic nerves within the prostate, and adjacent tissue can be imperceptible. Inadvertent injury to these thin or buried nerves is one of the most morbid but unintended consequences of surgery, which can lead to loss of function, numbness, and surgery induced neuropathic pain [1]. For example, radical prostatectomy (RP) can be performed for localized prostate cancer with excellent locoregional control [2, 3]. However, even with nerve-preserving radical prostatectomy there is a significant risk of erectile dysfunction and/or urinary incontinence, due to inadvertent injury to autonomic nerves or the autonomic neurovascular bundles [4, 5]. Preservation of the autonomic neurovascular bundles along the posterolateral aspect of the prostate is an important aspect for functional preservation during RP. The autonomic nerve fibers themselves are rarely visualized, but rather their position is presumed to track along vascular structures. The exact position and distribution of these autonomic nerves are variable from patient to patient, complicating the use of anatomical location as the sole method of avoidance [6-8] and injury can occur even in the most experienced hands. Recent studies showed that only 7% of RP patients regained pre-surgical state of full erectile function in the first year [9] and 16% regained baseline erectile function 2 years after prostatectomy [10].

Tools to improve visualization of the neural structures in the prostate have great potential for reducing morbidity from radical prostatectomy, as well as applications in many other nerve-preserving surgeries including cancer resection, trauma and reconstructive procedures. Systemic administration of a nerve imaging agent could allow the labeling of all relevant nerves with a single probe administration. Previously, reported methods rely on retrograde or anterograde tracing of individually axonal tracts by direct application of fluorescent dyes to the innervation site [11, 12]. Styryl pyridinium dyes [13-15], aminostyryl dyes [16-18], oxazine 4 [19, 20], and anti-ganglioside antibodies [21] have been investigated in various preclinical models to detect motor, sensory and autonomic nerves.

We previously identified a peptide sequence, Nerve Peptide 41 (NP41), through phage display that preferentially binds and highlights peripheral nerve tissue, enhancing visualization of motor and sensory nerves in live mice after systemic injection [22-24]. This peptide has relatively low affinity for nerve and rapid blood clearance (compared to antibodies) so it can be visualized a few hours after systemic injection with almost complete wash-out by 24 h [22]. NP41 has also been shown to highlight degenerate nerves through binding to structural laminins in nerve fibers [24, 25]. We have now used this peptide for intraoperative identification of autonomic nerves in the prostate of both mice and rats. To allow clinical translation of nerve visualization methods for use in surgeries involving human patients, we have now used phage display to identify a novel peptide HNP401 that, when labeled with a fluorophore, selectively binds and highlights human nerves. We show that fluorescently labeled HNP401 can bind to and highlight human sensory and motor nerves such as sural, medial antebrachial cutaneous, laryngeal, ansa cervicalis, great auricular nerve and autonomic nerves like those within and around the prostate gland.

Results

To visualize the autonomic nerves within the prostate of mice, we injected NP41 peptide conjugated to fluorescein (FAM-NP41) intravenously followed by imaging of prostate and surrounding tissue after surgical resection. Strong fluorescence from dye that rapidly accumulates in the bladder hindered visualization of the nerves within the prostate. To enhance visualization the bladder was surgically drained of urine and sutured prior to imaging. The urethra, an anatomically distinct structure, is never emptied of urine as the mice are alive for the duration of the experiment, resulting in a continuous passage of urine carrying metabolized peptide-dye to the bladder via the urethra. To aid future research, we have demonstrated using a fluorescence quenching dye (both directly injected in the bladder and through oral administration) to reduce high bladder fluorescence, as an alternative to surgical draining of the bladder (**Figure S1**). FAM-NP41 was injected at doses ranging from 150-600 nmol (~16-66 mg/kg) with a 600 nmol (~30 nmol/g) dose showing optimal autonomic nerve contrast (**Figure 1**). Low magnification fluorescence imaging shows highlighting of a single nerve fiber running adjacent to the urethra (**Figure 1A**). The nerve is extremely faint in a high magnification image using white light reflectance (**Figure 1B**) but becomes distinctly visible with FAM-NP41 labeling (**Figure 1C**). To quantify nerve detection, a total of 10 mice were injected with 600 nmol FAM-NP41 and signal intensity was measured for nerve versus adjacent non-nerve tissue using both fluorescence and white light reflectance. Values to the right of the line indicate that there is improved visualization with fluorescence compared to reflected light. Average nerve to non-nerve signal intensity with fluorescence guidance was 1.256 ± 0.14 (n=12,

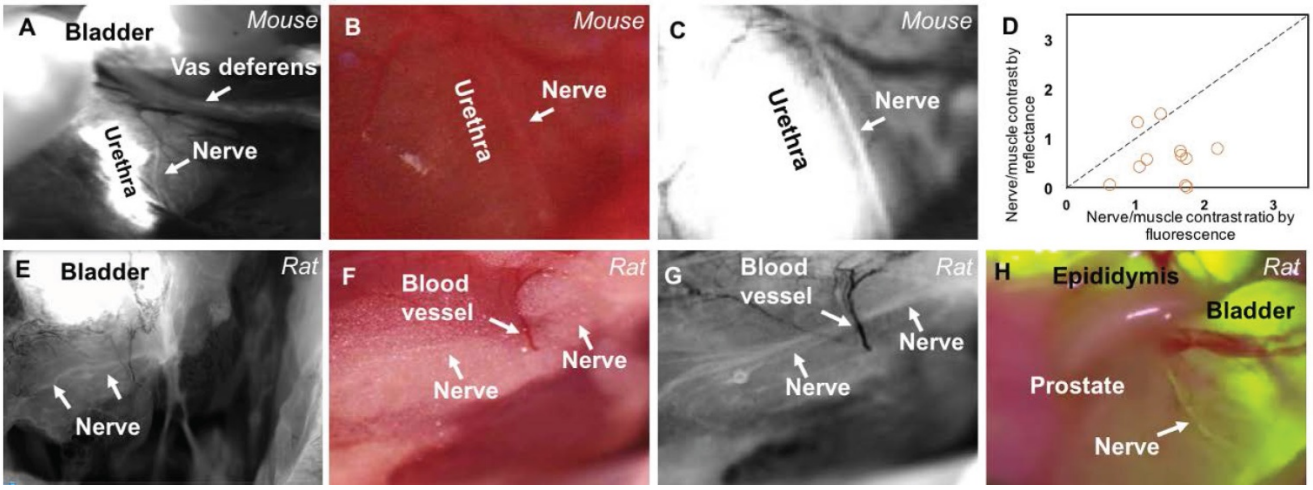

Figure 1. In-vivo fluorescent labelling of autonomic nerves in rodents. (A) Low magnification fluorescence image showing bladder, vas deferens and urethra running through the prostate with adjacent autonomic nerve labeled with FAM-NP41 in mice. Higher magnification white light reflectance image **(B)** and corresponding fluorescence grayscale image **(C)** of the autonomic nerve running adjacent to the urethra. Quantitation of autonomic nerve detection by fluorescence compared to white light detection in mice **(D)**. Nerve-to-muscle contrast for reflectance/fluorescence were plotted for individual nerve branches. Values to the right of the line indicate that there is improved visualization with fluorescence compared to reflected light. Images **(E-G)** are analogous to (A-C) except that they highlight FAM-NP41-dependent labeling of autonomic nerve in rat prostate versus mouse, with white light imaging showing non-visible nerve (F). **(H)** FAM-NP41-labeled prostate nerve is also detectable using a clinical grade Zeiss Pentero Surgical Microscope.

$p<0.001$) compared to 1.086 ± 0.07 (n= 12) for white-light reflectance (**Figure 1D**).

Because prostate nerves in mice were very small and challenging to image (i.e., requiring a high dose of FAM-NP41) we extended our study to the visualization of autonomic nerves within the prostate of rats. To visualize autonomic nerves in male Sprague Dawley rats, FAM-NP41 was injected intravenously at a dose of 12 nmol/g, followed by imaging. This is a 2.5x lower dose relative to weight compared to the 600 nmol used in 20 g mice. Useful labeling occurred 2-6 h after intravenous administration, which was visualized using a customized fluorescence dissecting microscope. FAM-NP41 nerve highlighting enables visualization of nerve fibers running through the middle of the rat prostate (**Figure 1E**). Higher magnification imaging showed that FAM-NP41 additionally highlighted autonomic nerve branches surrounding the neurovascular bundle (**Figure 1G**), which travel within the fatty capsule of the prostate gland. These branching nerves were not visible using white light reflectance imaging (**Figure 1F**). To quantitate selective labeling of autonomic nerves in rats, nerves within the prostate gland were imaged with both fluorescence and white light reflectance. Average nerve to non-nerve signal intensity from fluorescence was 1.275 ± 0.02 (n=3) compared to 1.083 ± 0.01 (n=3) for white light reflectance. To show applicability to intra-surgical imaging, we show that similar nerve contrast was observed in live rats using a clinical grade Zeiss Pentero imaging system (**Figure 1H**). The Zeiss Pentero scope, which is approved for clinical use, overlays the fluorescence image from FAM-NP41 (yellow) on the white light image with data collection in real time (**Figure 1H**). Recordings during surgical manipulation show fluorescent fibers within the prostate that clearly present as nerves that are detectable using NP41-FAM fluorescence guidance (**Video S1**). To confirm that the fluorescently labelled structures were indeed nerves, fluorescence surgical guidance was used in real time to selectively dissect out fluorescent fibers that were thought to be nerves (**Figure S2A**). Dissected fluorescent fibers were then positioned vertically and flash frozen in OCT embedding compound. Vertical cross sections were imaged using fluorescence to show that suspected nerve fibers were centered on slides (**Figure S2B**). Fibers were confirmed to be nerve as they were fluorescently labelled using dual immunohisto-chemically analysis with antibodies against either fluorophore (**Figure S2C**) or tyrosine hydroxylase (**Figure S2D**), a known marker for unmyelinated autonomic nerves. No immunostaining was detected in the absence of primary antibody (**Figure S2E**)

To enable translation of a nerve-illumination peptide for use in human patients, we performed phage display to identify human nerve-binding peptides using an m13 phage library expressing 16 random amino acid sequences on the N-terminus of gIII (Creative Biolabs). Phage were selected using iterative rounds of selection for binding to human sural nerve with negative selection to muscle and fat. Counter selection to muscles and fat was done by pre-absorbing the library with these tissues prior to selection for binding to human nerve. Individual phage were sequenced after each round of selection and three specific sequences, SGQVPWEEPYYVVKKS

(HNP401), WEYHYVDLNWTSQHPQ (HNP402), and DLPDIIWDFNWETAG (HNP403), were highly enriched after 5 and 6 rounds.

To test the affinity of the selected phage display peptides for binding to human nerves, they were chemically synthesized by solid-phase synthesis and labeled with fluorescein. Peptides were topically applied to sections of surgically harvested human sural nerve and temporalis muscle to determine nerve-to-muscle contrast for selected peptides and controls (**Figure S3**). Controls including free dye (carboxyfluorescein) were also tested on various nerves from multiple patient tissues to confirm specificity of peptide-dye conjugates for binding human nerve (**Figure S4**). We have shown that free non-reactive dye controls such as carboxyfluorescein show only weak non-specific binding and are not efficacious for topical applications. FAM-HNP401 yielded the highest contrast and was shown to be superior to the previously reported rodent nerve binding peptide FAM-NP41[22], when topically applied to human sural nerve (**Figure 2**). To quantify differential binding to nerve versus muscle, fluorescence signal intensity was measured for ROIs from the perineurium of select nerves and human temporalis muscle. FAM-HNP401 showed selective binding to human sural nerve with 10.9x fluorescence signal intensity (1374.44 ± 425.96) compared to FAM-NP41 (126.17 ± 61.03) (**Figure 2D**, p=0.009, Student's t-test, unpaired). Nerve-to-muscle contrast was comparable at 3.03 ± 0.57 for FAM-HNP401 and 2.28 ± 0.96 for FAM-NP41 (**Figure 2H**, p=0.236, Student's t-test, unpaired).

FAM-HNP401 was also tested topically on ex-vivo tissue for labeling mouse facial nerve with surrounding muscle, where it did not perform as well as FAM-NP41 (**Figure S5J-M**). For comparison, ex-vivo tissue labeling of human laryngeal nerve with surrounding muscle with FAM-NP41 and FAM-HNP401 is shown (**Figure S5F-I**). Autofluorescence of human nerve without treatment of peptide-dye conjugate was negligible compared to the signal intensity acquired after topical application of FAM-HNP401 (**Figure S6**). FAM-HNP401 also has a 2.3x higher signal intensity for in-vivo binding to mouse sciatic nerve compared to FAM-NP41 (**Figure 3A-C**). Nerve to surrounding muscle contrast was comparable for the two peptides (**Figure 3D**). FAM-HNP401 also highlighted rat sciatic nerve (**Figure 3E**) and prostate nerve (**Figure 3F**) at a dose of 2 μmol (~54 mg/kg) when imaged 3 h post injection. The bladder was drained with a syringe and sutured to avoid spillage and contamination around the prostate. The collected urine was analyzed by mass spectrometry and expected fragments of the peptide with dye attached were detected, indicating peptide in bladder was partially metabolized (**Figure S7**). Autonomic nerves within the prostate and adjacent to the vascular bundle could be easily visualized when imaged at higher magnification using a dose of 0.5

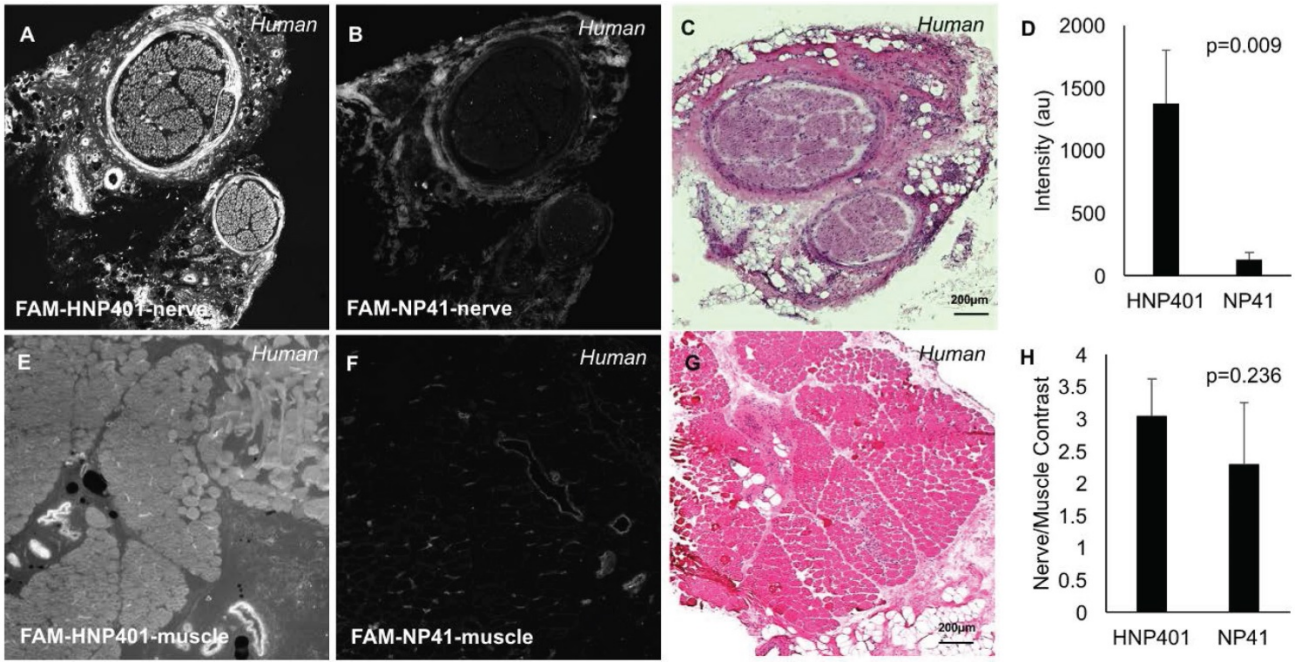

Figure 2. Comparison of FAM-HNP401 and FAM-NP41 in binding and labelling of human sural nerve. Topical application of 100 μM of FAM-HNP401 on 10 μm sections of unfixed human sural nerve tissue **(A)** and human temporalis muscle tissue **(E)** kept adjacent on the same glass slide and imaged on a confocal microscope with 488 nm laser excitation. For comparison, FAM-NP41 was applied to a sequential section of human nerve **(B)** and muscle **(F)** under identical conditions as for (A, E). H&E staining of the nerve **(C)** and muscle **(G)**. **(D)** Signal intensity of perineurium of nerve tissue treated with FAM-HNP401 (n=4) compared with FAM-NP41 (n=4). **(H)** Nerve-to-muscle contrast of peptides applied topically to human tissue sections (n=4).

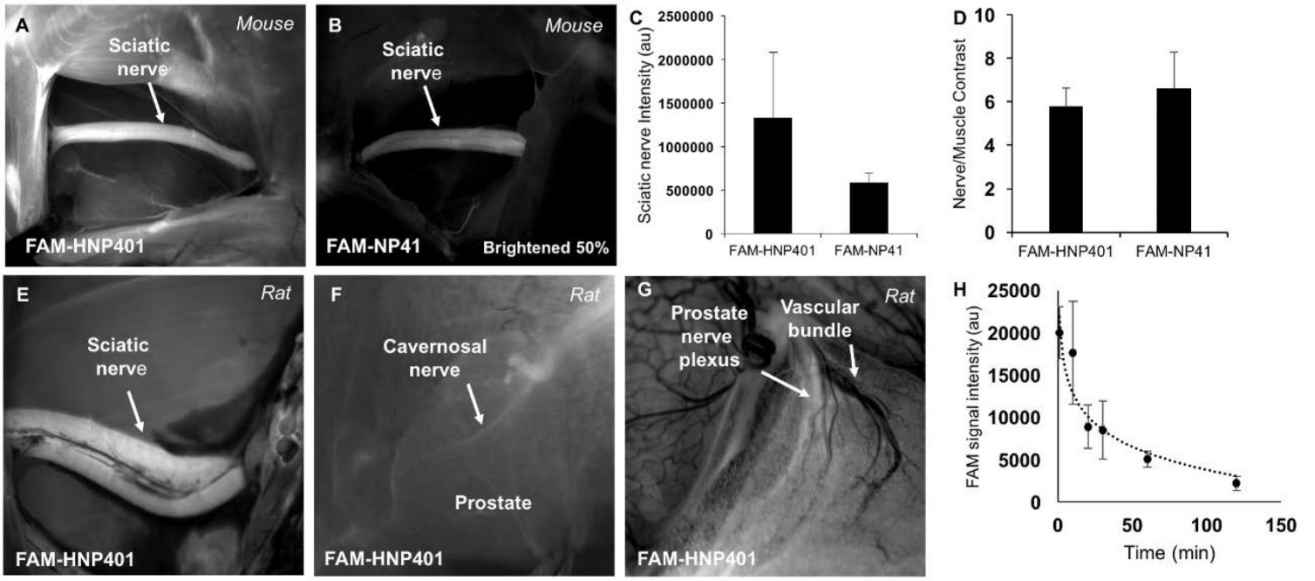

Figure 3. In vivo imaging of nerve-binding peptides in mice and rats with pharmacokinetics. In-vivo fluorescence images of sciatic nerves from 6-month-old SKH1 mice that had been previously intravenously injected with 450 nmol of FAM-HNP401 (~48.4 mg/kg) **(A)** or FAM-NP41 (~39 mg/kg) **(B)**. **(C)** The fluorescence intensity of the sciatic nerve measured and quantitated in Image J showed a 2.3-fold increase for FAM-HNP401 compared to FAM-NP41. **(D)** Nerve-to-muscle contrast for the two peptides were comparable at 5.79 ± 0.81 for FAM-HNP401 and 6.63 ± 1.63 for FAM-NP41. **(E)** In vivo fluorescence image of rat sciatic nerve 5 h after intravenous injection of 2 µmol of FAM-HNP401 (~54 mg/kg). Rat prostate nerve imaged with a real-time custom surgical imaging system **(F)** and Lumar small animal microscope **(G)** 5 h after intravenous injection of 2 µmol of FAM-HNP401. **(H)** The blood clearance curve shows FAM signal obtained from equal volume blood draws taken from five SKH1-Elite male mice. Each mouse was injected intravenously with 100 nmol (~11 mg/kg) of FAM-HNP401 prior to blood collection at 1 min, 10 min, 20 min, 30 min, 1 h and 2 h time points.

µmol (13.4 mg/kg) FAM-HNP401 10 min after probe injection (**Figure 3G**). Blood clearance of FAM-HNP401 showed a half-life of 30 min, which is similar to FAM-NP41 (**Figure 3H**). Optimal nerve contrast was detected using 50-100 µM (**Figure S5A-E**) with low concentration (10 µM) high resolution confocal imaging showing that FAM-HNP401 binds with high affinity to perineurium, epineurium and endoneurium while being excluded from axons (**Figure S5N**). FAM-HNP401 signal from human nerve saturates at 100 µM, while the signal from FAM-NP41 continues to increase even at 375 µM, but the signal intensity remains much lower than that of HNP401 applied at the same concentration (**Figure S5F-H**). The stability of FAM-HNP401 in human plasma at 5 min and 2 h was determined by incubation of the peptide-dye conjugate in human serum prior to analysis by mass spectrometry. For analysis, the area-under-the-curve at 450 nm and the corresponding mass of FAM-HNP401 were determined after injection of a fixed volume of analyte into the LC-MS (**Figure S8A-B**). For comparison, we also tested the stability of FAM-NP41 in human plasma (**Figure S7C-D**). Integration of the peak area at 5 min and 2 h indicates that both FAM-HNP401 and FAM-NP41 were stable in human serum. The area of extracted ion-current was used to determine peptide quantitation. No degradation of peptide-FAM conjugate was observed, with identical concentration detected at 5 min and 2 h of incubation with human plasma from analysis of the ion current. Peptides were analogously tested and shown to be stable in rat cerebrospinal fluid following 2 h exposure (**Figure S8E-F**).

FAM-HNP401 and FAM-NP41 were tested for binding to autonomic nerves, isolated from the prostate glands of two human patients (**Figure 4** and **Figure S9**). FAM-HNP401 (**Figure 4A** and **Figure S9A**) showed a significantly higher fluorescence signal in autonomic (cavernosal) nerves compared to FAM-NP41 (**Figure 4B** and **Figure S9B**). Quantitation was not done because only 2 patient samples were available for testing, as nerve resection during radical prostatectomy is only performed in instances of gross capsular invasion. Labelled fibers were confirmed as nerve using anti-neurofilament antibody SMI312 (red) with DAPI (blue) to show nuclear labeling (**Figure 4C**). H&E staining also confirmed the labeled tissue as nerve by histology (**Figure 4D**). SMI312 does not stain perineurium due to the lack of neurofilament fibers in this region of the nerve bundle. SMI312 staining shows that the tissue isolated is nerve due to staining of neurofilament structures that support the axons. Similar staining using FAM-HNP401 was obtained for another sensory nerve (anti-brachial cutaneous) isolated from human arm, showing the broad nerve-binding activity of HNP401 (**Figure 4E-H**).

To optimize and attempt to determine the core binding domain of HNP401, we performed systematic deletion of two amino acids from the C or N terminus (**Table S1**) followed by binding analysis on human sural nerve sections (**Figure 5**). In each case, nerve

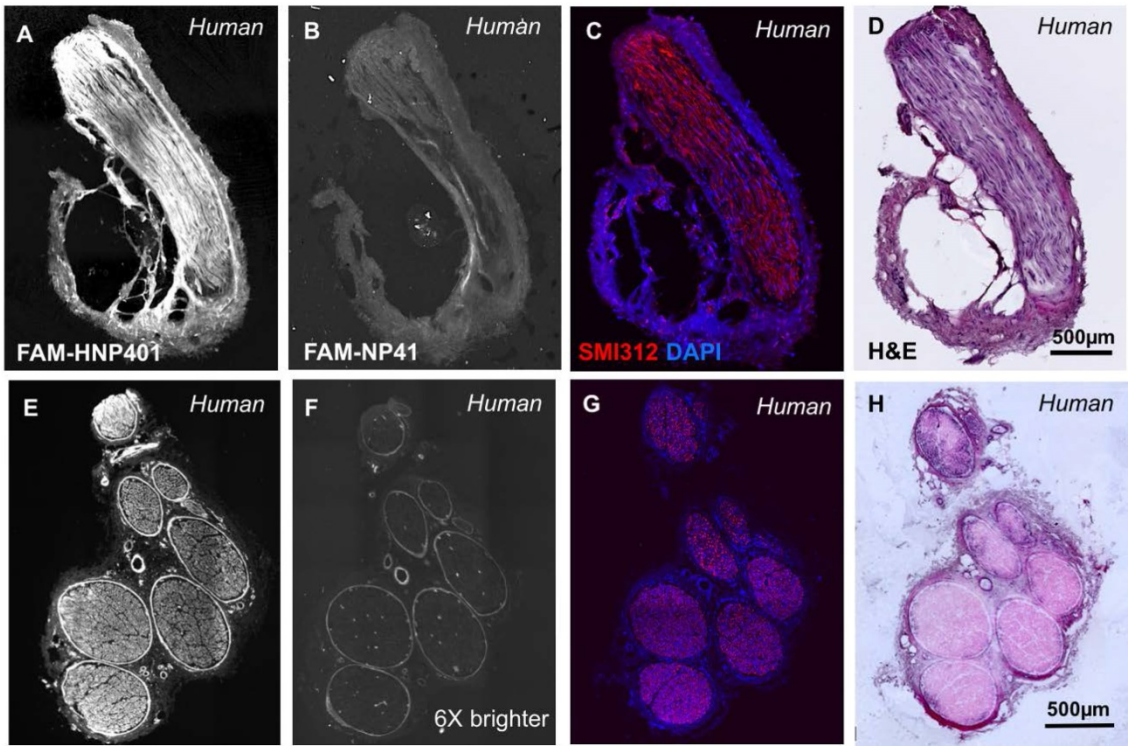

Figure 4. HNP401 binds to fresh viable nerve from the prostate gland and median anti-brachial cutaneous human nerve. Fluorescence imaging after topical application of 100 µM FAM-HNP401 or FAM-NP41 on 10 µm sections on cryosectioning tape of nerve within human prostate gland, **(A-B)** or from median anti-brachial cutaneous human nerve **(E-F)**. Nerves were imaged immediately after sectioning and application of peptide using confocal microscopy. Immunohistochemistry analysis with dual labelling for neurofilament antibody SMI312 (red) and DAPI-stained nuclei (blue) **(C, G)** and corresponding H&E staining **(D, H)** of a fixed section of nerve on glass slides.

binding and signal intensity was normalized to the parent FAM-HNP401 peptide (**Figure 5J**). Removal of the C-terminal serine (C-2) was tolerated, but upon removal of lysine (C-4) the solubility and binding was reduced dramatically with a normalized average signal intensity of 0.49 ± 0.11 for nerve binding of HNP401-C-4 (**Figure 5F**). Deletion of amino acids from the N terminal was mostly well tolerated. Removal of the N-terminal serine and glycine improved nerve selective binding about 2-fold with a normalized average signal intensity of 2.02 ± 0.65 for HNP401-N-2 (**Figure 5A, J**, p=0.026, Student's t-test, unpaired, one-tail). HNP401-N-4 has non-polar amino acids on its N-terminus, which reduced binding to a normalized average signal intensity of 0.56 ± 0.18 (**Figure 5B**). Removal of non-polar amino acids, tryptophan and proline, restored some binding intensity back to levels of FAM-HNP401, with HNP401-N-6 (**Figure 5C**) and HNP401-N-8 (**Figure 5D**) having normalized average nerve signal intensities of 1.0 ± 0.34 and 0.98 ± 0.31. The restored binding efficiency may be due to improved solubility minimizing micro-aggregation that occurs when very hydrophobic residues are present at the N terminus of a peptide. C and N terminal deletion studies of HNP-401 indicate the core binding domain likely includes PYYVVKK, with the N-terminal residues QVPWEE contributing to the enhanced binding detected with HNP401-N-2. Normalized nerve-to-temporalis muscle contrast for HNP401-N-2 gave a 3-fold increase with respect to FAM-HNP401 (**Figure 5K**, p=0.011, Student's t-test, unpaired, one-tail).

Discussion

Various tracer substances have long been used to map the connectivity in the nervous system, although most of them have depended on anterograde or retrograde tracing after local application [11, 12, 26, 27]. Transport of tracers is relatively slow, with contrast developing as dye moves away from the injection site [26, 27]. It is likely impractical to label the large areas exposed for surgeries by using these methods as multiple nerve tracts would have to be identified and independently labelled. There are reports of tracking retrograde neurovascular bundle and major pelvic ganglion with lipophilic dyes in rodents [4, 28]. More recently, styryl pyridinium dyes [13-15], aminostyryl dyes [16-18], oxazine 4 [19, 20], and anti-ganglioside antibodies [21] have been investigated in various preclinical models to detect motor, sensory and autonomic nerves. Dyes alone have no selective mechanism for nerve targeting but typically accumulate in the myelin. Myelin is known to be present in low abundance or be absent in autonomic nerves, which could limit the use of free dyes to highlight these fine but crucial nerves [29, 30].

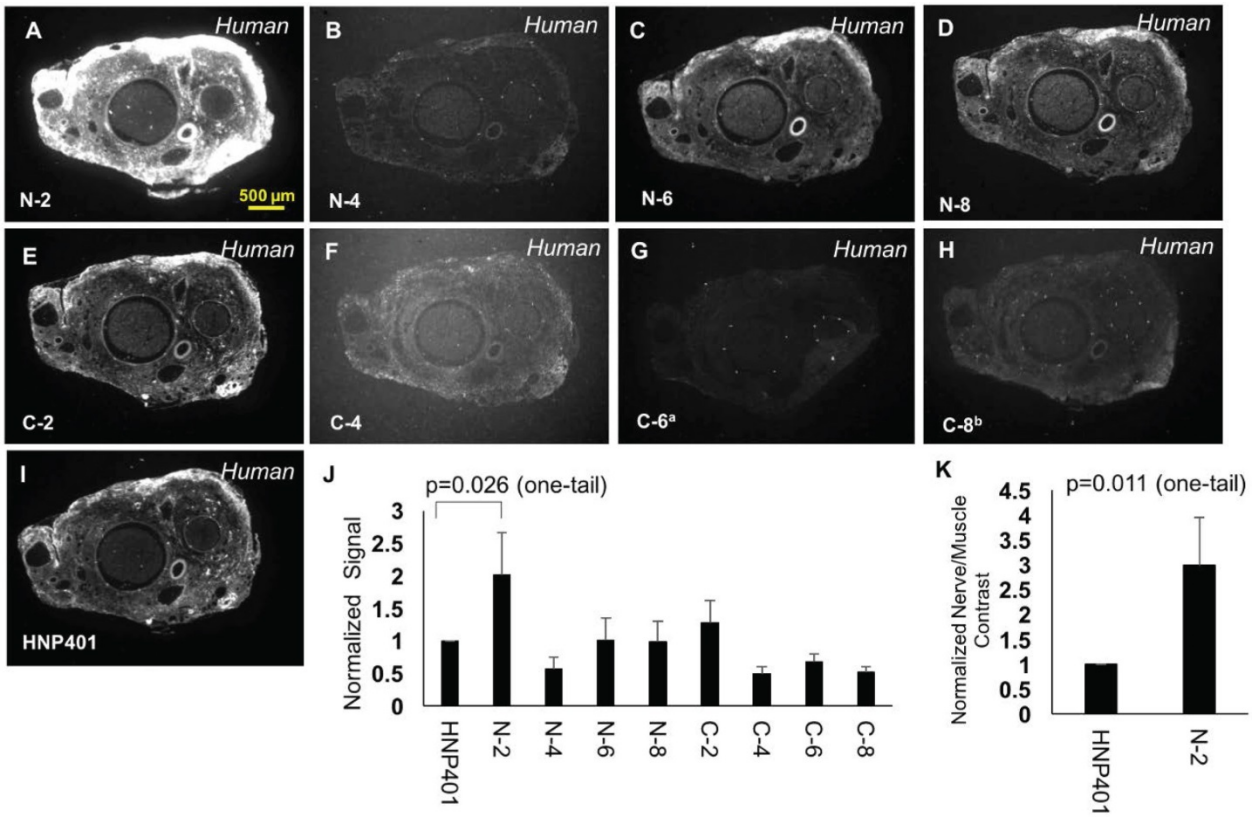

Figure 5. Comparison of truncated sequences to determine binding efficiency. Representative fluorescence images of unfixed human sural nerve that were treated topically with 100 µMof FAM-labelled N-2 **(A)**, N-4 **(B)**, N-6 **(C)**, N-8 **(D)**, C-2 **(E)**, C-4 **(F)**, C-6 **(G)**, C-8 **(H)** or HNP401 **(I)**. Due to poor solubility, C-6 had a final concentration of [a]73 µM and C-8 had a final concentration of [b]80.6 µM for topical tests. **(J)** Comparison of signal intensity of peptides normalized to FAM-HNP401 were made to test for improved binding. **(K)** Normalized sural nerve to temporalis muscle contrast was determined for FAM-HNP401 and FAM-HNP401-N-2 (Student t-test, unpaired, one-tail, p=0.011).

Topical and epidural application of free dyes has been used to locally label nerves in animal models; however, these approaches may be limited in flexibility during human surgeries as tissue is removed and the field of view changes [20, 31]. Anti-ganglioside antibodies have specific targeting but have long blood half-lives, which would likely require injection multiple days before surgery and may be more likely to elicit an immune response [32, 33]. Systemic injection of fluorescently labeled peptides to label nerves overcomes the major disadvantages of these tracers by labeling all nerves in the body with a single injection of peptide-dye conjugate. We previously reported on NP41 for binding rodent motor and sensory nerves and now demonstrate its potential application to the identification of fine autonomic nerves in rodent models. We found an average increase of 17% in nerve-to-non-nerve signal using fluorescence imaging compared to contrast obtained by white light reflectance. This is a significant accomplishment given the unmyelinated nature of these nerves and their ultra-fine structure. However, topical application of NP41 to human ex-vivo provided little contrast compared to muscle. To enhance highlighting of human nerves, we have now identified HNP401, a novel peptide that binds to and highlights human motor/sensory and autonomic nerves.

We expect the FAM-HNP-401 or an optimized analog could enable clinical translation of nerve visualization methods for use in surgeries involving human patients. Fluorescently labeled HNP401 can bind and highlight human sural, medial antebrachial cutaneous, laryngeal and autonomic nerves within and around the prostate gland. FAM-HNP401 showed high signal intensity and reproducible labelling of nerve bundles compared to its dye control of carboxyfluorescein. Carboxyfluorescein shows low signal and non-specific binding to nerve on topical human nerve sections. Dyes such as FITC-isothiocyanate cannot be used as the control as they will react with all nucleophilic side chains of proteins exposed by cross-sectioning in unfixed tissue. Additionally, FITC-dextran, although clinically used, is not a viable control for our experiments as it labels vasculature including micro blood vessels deep within the nerve cross section and is a marker for nerve injury and neuropathic pain [34]. In addition, its large size affects the pharmacokinetic profile of the dye. FAM-HNP401 consistently gave 10-fold higher

signal for binding human nerve compared to our previously identified FAM-NP41 peptide-dye conjugate. Higher signal intensity is an advantage for real-time imaging requiring short exposure times. HNP401 also showed a 3-fold contrast for nerve to muscle on topical sections in human ex-vivo tissue. FAM-HNP401 has a blood clearance profile similar to NP41 in mice [22]. FAM-HNP401 binds to myelinated and unmyelinated nerves. SMI312 antibody, which labels neurofilament, did not colocalized with FAM-HNP401 staining, demonstrating that FAM-HMP401 does not bind axons, but preferentially binds the perineurium, and therefore may be less likely to affect nerve conductivity. It is this staining pattern that leads us to believe HNP401-FAM is binding structural protein(s) in the perineurium. Polar amino acids at the C terminus appear to be needed for both solubility and binding as removal of either caused the peptide to become significantly less soluble or show decreased binding affinity to nerves. Removal of 2 amino acids on the N terminus increased nerve binding but further deletions negatively affected both solubility and binding. Attaching solubilizing groups like short pegs may restore binding to truncated variants.

In our initial studies, nerve-highlighting peptide HNP401 was coupled to a fairly short wavelength fluorescein derivative to make it compatible with dual nerve/tumor imaging using Cy5/Cy7 ratiometric activatable cell-penetrating peptides, which are currently in phase II clinical testing for detection of cancer (NCT03113825). Longer wavelength IR or near-IR dyes such as indocyanine green (ICG) or IRdye800 would potentially allow nerves to be imaged deeper below the surface in surgically exposed tissue after attachment to HNP-401. Free oxazine 4 has also been recently used to highlight nerves in preclinical models, and targeting could be enhanced by coupling to targeting peptides like HNP401. Although our preferred method of application is systemic, topical application is an option with some procedures. Such topical application of dye to the exposed surface followed by a washing to remove unbound dye has been used to image nerves in animal models [20]. Dyes such as 4-di-2-asp have also been used for topical application to nerves, but it has the disadvantage of being toxic to nerves due to its binding to mitochondria in nerve terminals [35]. Antibodies can be applied intravenously or topically and have some advantages including high affinity and a defined binding target; however as reported with the anti-ganglioside antibody, they require long circulation times for accumulation and washout to develop optimal nerve contrast.

In in vivo rodent studies, we found that peripheral motor and sensory nerves can be labeled in mice at a dose of 150 nmol FAM-NP41, which would easily scale to human dosing [36, 37]. Autonomic nerve labeling required a significantly higher dose in mice (600 nmol), so higher affinity peptides like HNP401 or improved variants may be required for advancement to clinical dosing. Interestingly, although higher dosing was required to visualize very small autonomic nerve in rodents (as small as 50 μm), labeling of significantly larger human prostate nerves (~750 μm) may be accomplished at a significantly reduced dose. Consistent with the conclusion that larger nerves can be highlighted with a lower dose, we were able to visualize nerves in rat prostate with a 40% dose NP41. Neither NP41 nor HNP401 permanently or covalently bind to nerve bundles as they both washed out with little remaining signal after 24 h. Structural proteins including laminins 421 and 211 have been identified as the binding targets for NP41[25]. While the binding targets for HNP401 have yet to be determined, imaging data shows a non-axonal binding pattern similar to NP41, indicating it may also bind structural nerve proteins. One significant characteristic of HNP401 compared to lipophilic dyes is that it does not require the presence of myelin and we have shown that it can bind and highlight the neurovascular bundle as well as the cavernosal nerve within the prostate. These nerves are important in urological applications and do not have high levels of myelination [29, 30]. We anticipate that preservation of nerves in this context represents one of the most urgent unmet clinical needs [38] for nerve imaging technology. The ability of FAM-HNP401 to highlight these nerves represents a significant advantage over competing nerve-binding agents that are selective for myelin [39] and incorporate into axons [21].

In addition to carrying dyes to highlight nerves for image-guided surgery, we envision the use of short nerve-binding peptides as carriers for therapeutics agents. Such conjugated systems might facilitate repair/regeneration of damaged nerves both in the periphery nervous system and in the spinal cord. The small size of nerve peptides like HNP401 also make them ideal for coating nanoparticles or dendrimers for delivering large payloads of drugs or imaging agents to the nervous system. NP41 serves as a useful agent for tracking mouse nerve in live animals requiring rapid binding and clearance of the agent. However, we expect that HNP401 or an optimized variant could have tremendous impact on patient outcomes by helping surgeons identify nerves prior to their exposure during surgery. The high signal intensity of HNP401 nerve highlighting should

enable nerve visualization with less sensitive wide-field imaging systems used during open surgery to reduce inadvertent nerve injury and post-surgical patient morbidity.

Methods

Probe synthesis

FAM-NP41 was synthesized as previously described [22]. A Prelude peptide synthesizer and standard Fmoc solid phase peptide synthesis was used to generate peptides with sequences acetyl-SGQVPWEEPYYVVKKSSGGCCONH$_2$ [HNP401], acetyl-WEYHYVDLNWTSQHPQGGC-CONH$_2$ [HNP402], and acetyl-DLPDIIWDFNWETAGGC-CONH$_2$ [HNP403]. Carboxyfluorescein was conjugated to the C-terminal cysteine using 5-fluorescein-maleimide [Anaspec] in the presence of N-methylmorpholine in DMSO. Peptides were purified on Agilent LCMS using a Phenomenex 5 µm C18 Luna with mass and purity > 95% confirmed by LC-MS. Truncated HNP401 peptides as listed in **Table S1** were synthesized and purified using the same configuration and method described above.

Animals

Wild-type male SKH1 mice (Charles River, Wilmington, MA) weighing 20-30 g were used for testing of peptide-dye conjugates. Male Sprague-Dawley rats weighing 100 to 250 g were used for in vivo testing of dye conjugates with the dose adjusted based on animal size. Protocols for the use of animals were approved by the Institutional Animal Care and Use Committee at University of California San Diego (Protocol number S05536).

In vivo imaging

Following anesthesia with intra-peritoneal injection of ketamine (80 mg/kg) and midazolam (40 mg/kg), FAM-NP41 or its variants were administered into mice retro-orbitally. After a washout period of 2-4 h, the animals were anesthetized with ketamine (50 mg/mL) and xylazine (20 mg/mL). The bladder and prostate were exposed through a midline abdominal incision. The autonomic nerve along the cavernosal vessel in the prostate was imaged and recorded using a custom-made surgical imaging system. This system is modified from an Olympus MVX10 scope capable of high-resolution fluorescence, RGB reflectance and real-time overlay with zoom from 0.6 to 5.7 cm field-of-view. ImageJ was used for quantitative analysis of nerve contrast for each peptide-dye conjugate tested. Images of autonomic nerve in prostate were selected from the recorded files and magnified 300-400% prior to selection of the ROI and measurement. Nerves and adjacent non-nerve tissue ROIs were hand-selected using the polygonal selection tool at the same location from both reflectance and fluorescence images. The mean and standard deviation of the pixel intensities within the selected areas were compared for nerves (mean = I_n, SD = σ_n) and adjacent background tissue (mean = I_b, SD = σ_b). Nerve-to-non-nerve contrast was calculated after background subtraction with the formula $|I_n - I_b| / (\sigma_n^2 + \sigma_m^2)^{0.5}$. For imaging the nerves in the prostate gland of male rats, peptide-dye conjugate were injected retro-orbitally. FAM-HNP401 was injected at a concentration of 13 mg/kg followed by imaging after 15 min, or, alternatively, a dose of 52 mg/kg was used with imaging after 3 h. Live animal surgery was performed under a ketamine-xylazine cocktail according to IACUC protocol. Sterile technique was used to expose the prostate; the bladder was drained with a small syringe and sutured. The surgical field was washed with sterile saline prior to imaging. Mann-Whitney test was used to analyze data for both mice and rats to compare nerve intensity and nerve-to-non-nerve contrast between white light reflectance and fluorescence images.

Confocal imaging parameters

Confocal data for **Figure 2** was acquired for 10 µm sections on glass using a 488 nm laser line and 10x magnification 0.45 NA air objective lens. The gain was set to 50, power was 0.5% of the laser power, pixel dwell time was 1.2 µs, aperture size was 1.2 µm, pixel size was 0.26 µm/px, and image size was 2k × 2k. We used the Nyquist feature and acquired images as tiles to get maximum resolution.

Confocal data for **Figure 4A and B** was acquired for 10 µm sections on glass using a 488 nm laser line and 10x magnification 0.45 NA air objective lens. The gain was set to 40, power was 3% of the laser power, pixel dwell time was 1.2 µs, aperture size was 1.2 µm, pixel size was 0.26 µm/px, and image size was 2k × 2k. We used the Nyquist feature and acquired images as tiles to get maximum resolution.

Confocal data for **Figure 4E and F** was acquired for 10 µm sections on glass using a 488 nm laser line and 10x magnification 0.45 NA air objective lens. The gain was set to 40, power was 1% of the laser power, pixel dwell time was 1.2 µs, aperture size was 1.2 µm, pixel size was 0.3 µm/px, and image size was 2k × 2k. Nyquist feature was not used.

Confocal data for SMI312 neurofilament antibody and Dapi staining were imaged at 10x magnification, 0.45 NA air objective lens with gain of 50, power of 5% of laser power for 405 nm laser line and gain of 100, power of 50% of laser power for 640 nm laser line. We used a pixel dwell was 3.2 µs,

aperture size was 1.2 µm and image size was 2k by 2k per tile resulting in a pixel size of 0.29 µm/px. We used the Nyquist feature and acquired images as tiles to get maximum resolution. Confocal data for **Figure S6** was acquired for 10 µm sections on glass using a 488 nm laser line and 10x magnification 0.45 NA air objective lens. The gain was set to 40, power was 3% of the laser power, pixel dwell time was 2.4 µs, aperture size was 1.2 µm, pixel size was 0.3 µm/px, and image size was 2k × 2k. Nyquist feature was not used.

Dose response data set of FAM-HNP401 on human nerve tissue (**Figure S5A-E**)was acquired for 10 µm sections on glass using a 488 nm laser line and 10x magnification 0.45 NA air objective lens. The gain was set to 40, power was 3% of the laser power, pixel dwell time was 1.2 µs, aperture size was 1.1 µm, pixel size was 0.3 µm/px, and image size was 2k × 2k. Nyquist feature was not used.

Confocal data for **Figure S9** was acquired for 10 µm sections on glass using a 488 nm laser line and 25x magnification 1.10 NA water immersion lens. The gain was set to 40, power was 3% of the laser power, pixel dwell time was 2.2 µs, aperture size was 1.2 µm, pixel size was 0.11 µm/px, and image size was 2k × 2k.

Phage display

Phage display was done using a custom-synthesized m13 phage library (diversity ~10^9) expressing 16 random amino acids on the N-terminus of gIII (Creative Biolabs). The phage library was processed through selections for binding to freshly resected or frozen human nerves, as was similarly described for the identification of NP41 that bound mouse nerves [22]. The library was processed through up to 6 binding and washing cycles. Prior to positive selection, phage were counter-selected for high-affinity muscle and fat tissue binding by pre-adsorbing the tissues with the library. For positive selection, phage libraries were mixed directly with human sural nerve tissue and incubated for up to 2 h at 4 °C. Following incubation, tissue phage mixtures were centrifuged and washed with PBS. Tissue pellets with bound phage were then homogenized, mixed with TG1 bacteria and plated on LB agar plates. Colonies were counted to determine titer followed by selecting single colonies for DNA preparation and sequencing. After each round of selection, phage were pooled and amplified for iterative selection. Phage that were bound at each round were sequenced and repeats noted. Duplicate phage as shown in the results were identified after 5 and 6 rounds of selection.

Topical application on tissue sections and imaging

Human sural nerve, antebrachial nerve and laryngeal nerve and temporalis muscle were obtained under IRB protocol number 130837 for Dr. Quyen Nguyen. Human peripheral nerves (typically sural) were obtained from patients undergoing nerve resection procedures. Human nerves from the prostate gland of two patients were acquired under Moores Cancer Centre Biorepository IRB protocol number 090401. Tissues were sectioned and mounted on glass slides or Cryojane tape. Tissue sections were placed in a humidifier chamber for 30 min before application of the peptide solution. Peptides were diluted to the appropriate concentration in 0.5X HBSS prior to topical application. 50 µL of peptide solution of known concentration (1 µM to 375 µM) was applied to 10 µm nerve sections on tape or slides and incubated for 30 min in a humidifier chamber. After incubation with peptide nerve, sections were washed twice with 0.5X HBSS and once with 1X PBS. A cover-slip was applied and slides were imaged immediately on either a Zeiss Lumar dissecting scope or a Nikon A1 confocal microscope. For confocal imaging, tissue sections of 10 µm thickness were imaged with a 488 nm laser excitation and 515nm/25nm band pass emission filter using a 10x air objective at a 0.26 µm/pixel resolution. For immunohistochemistry the confocal images were acquired with a 20x air objective at a resolution of 0.4 µm/pixel.

Image analysis

Image J was used to analyze and compare images acquired using the confocal microscope and the Lumar dissecting scope. For each experimental set where probes were compared, we kept the acquisition parameters identical so as to directly compare the data obtained. During the experiment, it is clear that FAM-HNP401 had the brightest signal in our topical application experiments. All raw image files for a given experimental cohort were loaded at the same time into Image J as 16-bit tiff images. We then levelled the images for tissue treated with FAM-HNP401. Once these levels were set, the settings were propagated to all images in one step using Image J. The brightest image was set as the benchmark for all other images in the cohort to avoid saturating when the leveling was propagated. For quantifying the images, regions-of-interest (ROI) were drawn and the signal counts measured in image J. For **Figure 5**, even though FAM-HNP401-N-2 was the brightest, for consistency we choose FAM-HNP401 to level and normalize signal counts.

Immunofluorescence of autonomic nerves from rat prostate

Suspect unmyelinated nerve tissue was taken from the prostate gland of male rats after in vivo intravenous injection of TAMRA-NP41 (0.5 μmol or 11.3 mg/kg for 100 g rats) visualized on a custom-made surgical fluorescence imaging system based on an Olympus dissecting microscope. 5 μm cryosections of the tissue were generated using a Leica Cryostat and mounted on Cryojane tape. Tissue sections were fixed for 10 min with 4% para-formaldehyde in 1X PBS followed by a 1X PBS rinse. A 1:2000 dilution of monoclonal antibody against TAMRA (Thermofisher Scientific Cat. No. MA1-041) or polyclonal antibody against tyrosine hydroxylase (Cell Signaling Technologies Prod. No. 2792S) in 10 % goat serum in PBS was applied (20 μL per section) and incubated overnight at room temperature followed by a 1X PBS wash. A 1:500 dilution of biotinylated anti-mouse secondary antibody was applied in 10% goat serum in PBS to sections for 2 h followed by a 1X PBS wash. Vector RTU (avidin biotin complex) or Alexa 405 streptavidin was applied for 1 h followed by a 1X PBS wash. Tissue was wet-mounted on slides with 1X PBS. Confocal images were acquired with a 20x air objective at resolution of 0.4 μm/pixel.

Immunofluorescence for neurofilament

Fresh viable human nerve tissue was obtained from prostatectomy and frozen in OCT blocks. 10 μm cryosections of tissue were mounted on glass True Bond slides. Hydrophobic barrier pen was applied to the glass around each section. Tissue sections were fixed using 2% paraformaldehyde prepared in 1X PBS and washed 4 times with 1X PBS. 100 μL of blocking buffer (0.01% Triton X solution, 1% BSA in 10% normal goat serum (Life technologies 50062Z)) was applied for 30 min to each tissue section. The tissue was then washed 4 times with 1X PBS and a 1:1000 dilution of neurofilament SMI312 antibody (Biolegend Cat. No. 837904) was applied to the tissue for overnight incubation at 4 °C. Tissues were washed 6 times with PBST. A 1:1000 dilution of anti-mouse secondary antibody AlexaFluor 555 was applied to the sections for 2 h at 4 °C followed by washing with 1X PBS. Prolong Gold Anti-fade reagent with DAPI (Life Technologies P36931) was added prior to cover slipping and imaging.

H&E staining protocol

Tissue sections were fixed for 1 min in 1:1 10% buffered formaldehyde and 200 proof ethanol. Slides were then washed with water and immersed in hematoxylin stain for 2 min. Slides were then washed with distilled water and immersed in bluing solution for 30 s. Slides were washed with distilled water and immersed in eosin solution for 1 min followed by washing with distilled water. Slides were sequentially dipped in 50%, 95% and 100% ethanol to remove water. Slides were air dried and dipped in citrisolv before mounting a cover-slip with non-xylene mounting solution and imaging on a Hamamatsu Nanozoomer using bright-field imaging at 20x magnification.

Blood clearance for HNP401-FAM

Five 8-week-old SKH male mice were injected intravenously with 100 nmol (10.75 mg/kg for 25 g mice) of FAM-HNP401 in 100 μL of sterile water. Prior to blood draw, mice were anesthetized with a 1:1 cocktail of ketamine: midazolam. Tail pricks were performed at 1 min, 10 min, 20 min, 30 min, 1 h, and 2 h after injection to collect 5 μL whole blood, which was dissolved in 100 μL Agilent ICP-MS tuning buffer. Samples were centrifuged and equal volumes of supernatants were analyzed using a Tecan fluorescence plate reader.

Supplementary Material

Supplementary figures and table.
http://www.thno.org/v08p4226s1.pdf

Acknowledgements

The authors would like to thank Susie Johnson for assistance with animal experiments and Paul Steinbach for computational and imaging support. This study was supported by R01 EB014929-05 to Drs. Quyen T Nguyen, Michael A Whitney and Roger Y Tsien. Dr. Roger Tsien, passed away during the preparation of this manuscript.

Competing interests

Dr. Quyen T Nguyen and Dr. Michael A Whitney are founders of Alume Biosciences, Inc. which is currently licensing technology from UC San Diego.

References

[1] Borsook D, Kussman BD, George E, Becerra LR, Burke DW. Surgically induced neuropathic pain: understanding the perioperative process. Ann Surg. 2013; 257(6): e403-12.
[2] D'Amico AV, Whittington R, Malkowicz SB, Schultz D, Blank K, Broderick GA, et al. Biochemical outcome after radical prostatectomy, external beam radiation therapy, or interstitial radiation therapy for clinically localized prostate cancer. JAMA. 1998; 280(11): 969-74.
[3] Walsh PC. Radical prostatectomy for localized prostate cancer provides durable cancer control with excellent quality of life: a structured debate. J Urol. 2000; 163(6): 1802-7.
[4] Yamashita S, Kato R, Kobayashi K, Hisasue Si, Arai Y, Tsukamoto T. Nerve injury related erectile dysfunction following nerve sparing radical prostatectomy: A novel experimental dissection model. Int J Urol. 2009; 16(11): 905-11.
[5] Stanford JL, Feng Z, Hamilton AS, Gilliland FD, Stephenson RA, Eley JW, et al. Urinary and sexual function after radical prostatectomy for clinically localized

prostate cancer: the Prostate Cancer Outcomes Study. JAMA. 2000; 283(3): 354-60.
[6] Walsh PC. Anatomic radical prostatectomy: evolution of the surgical technique. J Urol. 1998; 160(6 Pt 2): 2418-24.
[7] Tewari A, Peabody JO, Fischer M, Sarle R, Vallancien G, Delmas V, et al. An operative and anatomic study to help in nerve sparing during laparoscopic and robotic radical prostatectomy. Eur Urol. 2003; 43(5): 444-54.
[8] Nandipati KC, Raina R, Agarwal A, Zippe CD. Nerve-sparing surgery significantly affects long-term continence after radical prostatectomy. Urology. 2007; 70(6): 1127-30.
[9] Koehler N, Holze S, Gansera L, Rebmann U, Roth S, Scholz HJ, et al. Erectile dysfunction after radical prostatectomy: the impact of nerve-sparing status and surgical approach. Int J Impot Res. 2012; 24(4): 155-60.
[10] Nelson CJ, Scardino PT, Eastham JA, Mulhall JP. Back to Baseline: Erectile Function Recovery after Radical Prostatectomy from the Patients' Perspective. J Sex Med. 2013; 10(6): 1636-43.
[11] O'Malley MR, Wittkopf JE, Cutler JL, Labadie RF, Hackett TA, Haynes DS. Fluorescent retrograde axonal tracing of the facial nerve. The Laryngoscope. 2006; 116(10): 1792-7.
[12] Marangos N, Illing R-B, Krüger J, Laszig R. In vivo visualization of the cochlear nerve and nuclei with fluorescent axonal tracers. Hear Res. 2001; 162(1-2): 48-52.
[13] De Proost I, Pintelon I, Brouns I, Timmermans J-P, Adriaensen D. Selective visualisation of sensory receptors in the smooth muscle layer of ex-vivo airway whole-mounts by styryl pyridinium dyes. Cell Tissue Res. 2007; 329(3): 421-31.
[14] Naskar R, Wissing M, Thanos S. Detection of early neuron degeneration and accompanying microglial responses in the retina of a rat model of glaucoma. Invest Ophthalmo Vis Sci. 2002; 43(9): 2962-8.
[15] Papworth GD, Delaney PM, Bussau LJ, Vo LT, King RG. In vivo fibre optic confocal imaging of microvasculature and nerves in the rat vas deferens and colon. J Anat. 1998; 192(Pt 4): 489-95.
[16] Gibbs-Strauss SL, Nasr KA, Fish KM, Khullar O, Ashitate Y, Siclovan TM, et al. Nerve-highlighting fluorescent contrast agents for image-guided surgery. Mol Imaging. 2011; 10(2): 7290-2010.
[17] Cotero VE, Kimm SY, Siclovan TM, Zhang R, Kim EM, Matsumoto K, et al. Improved intraoperative visualization of nerves through a myelin-binding fluorophore and dual-mode laparoscopic imaging. PloS One. 2015; 10(6): e0130276.
[18] Stankoff B, Wang Y, Bottlaender M, Aigrot M-S, Dolle F, Wu C, et al. Imaging of CNS myelin by positron-emission tomography. Proc Nat Acad Sci USA. 2006; 103(24): 9304-9.
[19] Park MH, Hyun H, Ashitate Y, Wada H, Park G, Lee JH, et al. Prototype nerve-specific near-infrared fluorophores. Theranostics. 2014; 4(8): 823-33.
[20] Barth CW, Gibbs SL. Direct Administration of Nerve-Specific Contrast to Improve Nerve Sparing Radical Prostatectomy. Theranostics. 2017; 7(3): 573-93.
[21] Massaad CA, Zhang G, Pillai L, Azhdarinia A, Liu W, Sheikh KA. Fluorescently-tagged anti-ganglioside antibody selectively identifies peripheral nerve in living animals. Sci Rep. 2015; 5: 15766.
[22] Whitney MA, Crisp JL, Nguyen LT, Friedman B, Gross LA, Steinbach P, et al. Fluorescent peptides highlight peripheral nerves during surgery in mice. Nat Biotechnol. 2011; 29(4): 352-6.
[23] Wu AP, Whitney MA, Crisp JL, Friedman B, Tsien RY, Nguyen QT. Improved facial nerve identification with novel fluorescently labeled probe. Laryngoscope. 2011; 121(4): 805-10.
[24] Hussain T, Mastrodimos MB, Raju SC, Glasgow HL, Whitney M, Friedman B, et al. Fluorescently labeled peptide increases identification of degenerated facial nerve branches during surgery and improves functional outcome. PloS One. 2015; 10(3): e0119600.
[25] Glasgow HL, Whitney MA, Gross LA, Friedman B, Adams SR, Crisp JL, et al. Laminin targeting of a peripheral nerve-highlighting peptide enables degenerated nerve visualization. Proc Nat Acad Sci USA. 2016; 113(45): 12774-9.
[26] Köbbert C, Apps R, Bechmann I, Lanciego JL, Mey J, Thanos S. Current concepts in neuroanatomical tracing. Prog Neurobiol. 2000; 62(4): 327-51.
[27] Richmond FJR, Gladdy R, Creasy JL, Kitamura S, Smits E, Thomson DB. Efficacy of seven retrograde tracers, compared in multiple-labelling studies of feline motoneurones. J Neurosci Methods. 1994; 53(1): 35-46.
[28] Davila HH, Mamcarz M, Nadelhaft I, Salup R, Lockhart J, Carrion RE. Visualization of the neurovascular bundles and major pelvic ganglion with fluorescent tracers after penile injection in the rat. BJU Int. 2008; 101(8): 1048-51.
[29] Schaumburg HH, Zotova E, Cannella B, Raine CS, Arezzo J, Tar M, et al. Structural and functional investigations of the murine cavernosal nerve: a model system for serial spatio-temporal study of autonomic neuropathy. BJU Int. 2007; 99(4): 916-24.
[30] Karam I, Droupy S, Abd-Alsamad I, Korbage A, Uhl J-F, Benoît G, et al. The precise location and nature of the nerves to the male human urethra: histological and immunohistochemical studies with three-dimensional reconstruction. Eur Urol. 2005; 48(5): 858-64.
[31] Liu W, Gu R, Zhu Q, Xiao C, Huang L, Zhuang X, et al. Rapid fluorescence imaging of spinal cord following epidural administration of a nerve-highlighting fluorophore. Theranostics. 2017; 7(7): 1863-74.
[32] Descotes J. Immunotoxicity of monoclonal antibodies. MAbs. 2009; 1(2): 104-11.
[33] Chames P, Van Regenmortel M, Weiss E, Baty D. Therapeutic antibodies: successes, limitations and hopes for the future. Br J Pharmacol. 2009; 157(2): 220-33.
[34] Lim TKY, Shi XQ, Johnson JM, Rone MB, Antel JP, David S, et al. Peripheral nerve injury induces persistent vascular dysfunction and endoneurial hypoxia, contributing to the genesis of neuropathic pain. J Neurosci. 2015; 35(8): 3346-59.
[35] Marques MJ, Santo Neto H. Imaging neuromuscular junctions by confocal fluorescence microscopy: individual endplates seen in whole muscles with vital intracellular staining of the nerve terminals. J Anat. 1998; 192(Pt 3): 425-30.
[36] Cherrick GR, Stein SW, Leevy CM, Davidson CS. Indocyanine green: observations on its physical properties, plasma decay, and hepatic extraction. J Clin Invest. 1960; 39: 592-600.
[37] Marshall MV, Rasmussen JC, Tan IC, Aldrich MB, Adams KE, Wang X, et al. Near-infrared fluorescence imaging in humans with indocyanine green: a review and update. Open Surg Onco J. 2010; 2(2): 12-25.
[38] Guillonneau B. Neurological and vascular preservation during laparoscopic radical prostatectomy. Prog Urol. 2009; 19(Suppl 4): S180-2.
[39] Wang C, Wu C, Zhu J, Miller RH, Wang Y. Design, synthesis, and evaluation of coumarin-based molecular probes for imaging of myelination. J Med Chem. 2011; 54(7): 2331-40.